Dissection of the EntF Condensation Domain Boundary and Active Site Residues in Nonribosomal Peptide Synthesis[†]

Eric D. Roche and Christopher T. Walsh*

Department of Biological Chemistry and Molecular Pharmacology, Harvard Medical School, Boston, Massachusetts 02115

Received September 18, 2002; Revised Manuscript Received November 14, 2002

ABSTRACT: Nonribosomal peptide synthetases (NRPSs) make many natural products of clinical importance, but a deeper understanding of the protein domains that compose NRPS assembly lines is required before these megasynthetases can be effectively engineered to produce novel drugs. The N-terminal amide bond-forming condensation (C) domain of the enterobactin NRPS EntF was excised from the multidomain synthetase using endpoints determined from sequence alignments and secondary structure predictions. The isolated domain was well-folded when compared by circular dichroism to the vibriobactin NRPS VibH, a naturally free-standing C domain. The EntF domain was also fully functional in an assay based on a synthetic small-molecule substrate, seryl *N*-acetylcysteamine. Active site mutants of the EntF C domain were surprisingly inactive in vitro as compared to their VibH counterparts, yet maintained the overall domain structure. An in vivo assay was developed in the context of the full-length EntF protein to more sensitively probe the activity level of the C domain mutants, and this supported strong effects for the active site mutations. The crucial role of histidine-138 was confirmed by assay of the full-length protein in vitro. These results suggest a strong resemblance of catalysis by the EntF C domain to chloramphenicol acetyltransferase, including an active site organized by an arginine−aspartate salt bridge, a key histidine acting as a general base, and an asparagine instead of a serine stabilizing the proposed tetrahedral intermediate by hydrogen bonding. The precise definition of a functional C domain excised from a NRPS should aid efforts at swapping NRPS domains between assembly lines.

Nonribosomal peptide synthetases (NRPSs)[1] act as enzymatic assembly lines to produce many peptide antibiotics and peptide-based iron chelators (*1*−*5*). A central feature of these assembly lines is their modular organization with one protein module per amino acid selected, activated, and incorporated. Each module has a core set of catalytic domains and one peptidyl carrier protein (PCP) domain that is post-translationally modified by addition of a phosphopantetheine cofactor. The terminal thiol of this cofactor arm is the site of covalent attachment for the growing peptide chain in each module. The iterative organization of NRPSs has enabled limited swapping of NRPS modules and domains to produce new synthetases and products (*6*−*11*), but more extensive engineering for combinatorial biosynthesis requires a greater knowledge of domain boundaries, activities, and compatibility.

While there is great interest in reconstituting the multimodular NRPSs to generate new antibiotics, to date the only NRPS systems that have been fully reconstituted make siderophores (*12*−*16*). These small molecules are secreted by bacteria and then transported back into the cell after chelating iron. This iron acquisition strategy is essential for bacterial pathogenesis, as bacteria unable to produce siderophores fail to survive in hosts and under other conditions of iron scarcity (*1*). The inability of mutant *Escherichia coli* to grow on iron-poor media was used to identify the genes required for synthesis of the siderophore enterobactin (*17*, *18*). The corresponding protein assembly line, enterobactin synthetase, has been reconstituted at rates of 60−200 turnovers per minute from pure EntE, EntB, and EntF, properly phosphopantetheinylated on the two PCP domains (Figure 1A) (*14*).

The enterobactin synthetase has been a fruitful system for exploration of NRPS function, enabling some dissection of the many catalytic functions of such an assembly line. EntE selects and activates 2,3-dihydroxybenzoate (DHB) (*19*). EntB supplies a H*S*-pantetheinyl-PCP domain for generation of a DHB-*S*-EntB acyl enzyme intermediate from DHB-AMP bound to EntE (Figure 1A-2) (*20*). The EntF protein is of particular interest because the 140 kDa four domain catalyst is a complete module containing one of each of the core NRPS domains including condensation, adenylation, peptidyl carrier protein, and thioesterase domains: C−A−PCP−TE. The EntF A domain is believed to activate and load serine to form a seryl-*S*-PCP (Figure 1A-1) (*14*, *21*). The C domain

[†] This work was supported by National Institutes of Health Grants GM49338-08 and PO1-GM47467-11. E.D.R. is a Fellow of the Jane Coffin Childs Memorial Fund for Medical Research.

* To whom correspondence should be addressed. Phone: (617) 432-1715. Fax: (617) 432-0438. E-mail: christopher_walsh@hms.harvard.edu.

[1] Abbreviations: A, adenylation domain; AMP, adenosine monophosphate; ATP, adenosine triphosphate; ArCP, aryl carrier protein; C, condensation domain; CAS, chrome azurol S; CAT, chloramphenicol acetyl transferase; CD, circular dichroism; DHB, 2,3-dihydroxybenzoate; DTT, dithiothreitol; HPLC, high-performance liquid chromatography; LB, Luria−Bertani media; NRPS, nonribosomal peptide synthetase; NTA, nitrilotriacetic acid; PCP, peptidyl carrier protein; PCR, polymerase chain reaction; SNAC, *N*-acetylcysteamine thioester; TE, thioesterase domain; WT, wild-type.

10.1021/bi026867m CCC: $25.00 © 2003 American Chemical Society
Published on Web 01/04/2003

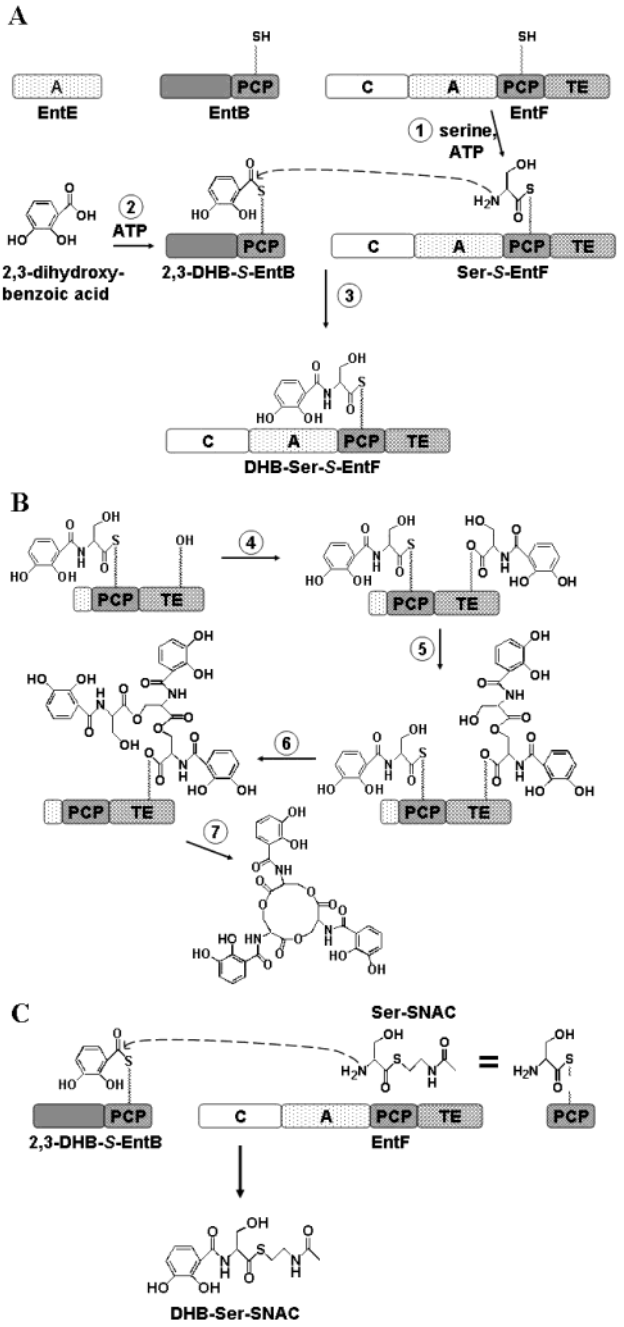

FIGURE 1: Catalytic steps on the assembly line formed by the two-module enterobactin synthetase composed of proteins EntE, EntB, and EntF. See text for details.

is thought to catalyze amide bond formation between DHB activated on EntB and seryl-*S*-EntF leading to a DHB-seryl-*S*-EntF acyl enzyme intermediate (Figure 1A-3) (*14*). The activity of the thioesterase domain has been probed by mutagenesis of the putative serine−histidine−aspartate catalytic triad, and the resultant intermediates provided support for the model shown in Figure 1B (*22*). Under this proposal, the TE domain in the course of cyclotrimerization must store successively DHB-Ser, $(DHB\text{-}Ser)_2$, and uncyclized $(DHB\text{-}Ser)_3$ acyl moieties, covalently bound on the TE domain (Figure 1B-4−6), prior to cyclization to produce the tri-catecholic siderophore (Figure 1B-7).

The C domain is imputed in this and other NRPS assembly lines to be the peptide bond-forming catalyst. With one C domain in every NRPS module that carries out a chain elongation step, the C domains are the fundamental iterative catalysts for peptidyl-*S*-enzyme chain growth. Because C domains are typically embedded in multidomain protein modules in high molecular weight protein subunits, they have been difficult to characterize structurally and functionally. The presence of a highly conserved HHxxxDG motif suggested a similarity between NRPS condensation domains and a superfamily of acyl transferases, including the well-characterized chloramphenicol acetyltransferase (CAT) (*23*, *24*). The second histidine is a key catalytic base for CAT function (*25*). Although mutagenesis of this histidine eliminates activity for one NRPS module involved in synthesis of the antibiotic tyrocidine, mixed results have been obtained from similar mutations in other synthetases (*26*−*29*). Thus, the degree of mechanistic similarity between NRPS C domains and CAT-like acyl transferases remains unclear.

As a step to evaluate C domain action in NRPS assembly lines, we developed an assay that turned the EntF C domain from a stoichiometric self-acylation catalyst (making DHB-Ser-*S*-EntF) into a multiple-turnover system providing increased sensitivity for product detection (*30*). The embedded 10 kDa H*S*-pantetheinyl-PCP domain was replaced by the small molecule H*S*-*N*-acetylcysteamine (HSNAC). Specifically, L-seryl-SNAC served as a surrogate acceptor substrate for EntF in the presence of DHB-*S*-EntB as a donor to yield DHB-Ser-SNAC, a product not covalently linked to the enzyme and therefore readily detected and quantified by HPLC (Figure 1C) (*30*). With this assay in hand, we have turned to expression and characterization of the predicted 50 kDa N-terminal C domain from the 140 kDa full-length EntF. During the course of this work, the structure of the vibriobactin synthetase subunit VibH, an unusual naturally free-standing C domain, was solved (*29*). On the basis of the structures of VibH and CAT (*31*), we have made mutants to evaluate the role of EntF C domain residues in amide bond formation and assayed them both in vitro and in vivo. The results suggest catalysis by the EntF C domain is mechanistically similar to CAT and provide groundwork for future domain-swapping and genetic manipulation.

EXPERIMENTAL PROCEDURES

Plasmid Construction. Oligonucleotides used to create strains and plasmids are listed in Table 1. The correct structure of plasmids was confirmed by DNA sequencing (Dana-Farber/Harvard Cancer Center High-Throughput DNA Sequencing Facility) and restriction enzyme digests. The EntF constructs generated by these studies have expression under T7 promoter control, include a kanamycin resistance gene, and produce EntF proteins bearing C-terminal His_6 tags. A C-terminal tag was chosen to protect the EntF truncations from degradation by proteases that recognize hydrophobic C-termini (*32*). Plasmids pER301 and pER302 for expression of EntF C(1−435) and C(1−425) domains were generated by PCR amplification of pMS22 (*21*) using primer EDR1.1 with either EDR1.2 or EDR1.3, followed by ligation of the appropriately digested products between the NdeI and the XhoI restriction sites of pET29. pER301 was digested with restriction enzymes BamHI and XhoI and ligated to annealed oligos EDR15.1 and EDR15.2 to yield plasmid pER315 expressing EntF C(1−432). The full-length EntF construct,

Table 1: Primers Used to Make Plasmids and Strain ER1100A[a]

primer	construct	sequence
EDR1.1	C(1−435), pER301	5′-gtccacgagcatatgagccagcatttacctttggt-3′
EDR1.2	C(1−435), pER301	5′-ccaaggctcgagcataatatcgacatcgccg-3′
EDR1.3	C(1−425), pER302	5′-gccttgctcgagcgccggatccgcggcgaact-3′
EDR15.1	C(1−432), pER315	5′-gatccggcgctgttgtgcggcgatgtcgatc-3′
EDR15.2	C(1−432), pER315	5′-tcgagatcgacatcgccgcacaacagcgccg-3′
EDR5.5	EntF, pER311	5′-ccttgctcgagacggtttagcgttgcgcgaataat-3′
EDR19.1	H138F,L,I,M,V	5′-gtactggtatcagcgttatcacDTKttgctggtc-3′
EDR19.2	H138S,P,T,A	5′-gtactggtatcagcgttatcacNCAttgctggtc-3′
EDR19.3	H138Y,Q,N,K,D,E	5′-gtactggtatcagcgttatcacNaKttgctggtc-3′
EDR19.4	H138C,R,G	5′-gtactggtatcagcgttatcacBGtttgctggtc-3′
EDR19.5	H138X	5′-gtgataacgctgataccagtacca-3′
EDR22.1	EntF⁻, ER1100A	5′-ccgacgaattttacccagttgcaggaggcacaatga gccagcatttacctgtgtaggctggagctgcttc-3′
EDR22.2	EntF⁻, ER1100A	5′-tctgtaattatgggtttataaatatattaatttacctgttt agcgttgccatatgaatatcctccttag-3′
EDR25.1	D142A	5′-tttgctggtcgCtggctttagt-3′
EDR25.3	D142N	5′-tttgctggtcAaTggctttagt-3′
EDR26.1	G143L	5′-tgctggtcgatCTctttagtttc-3′
EDR27.1	I14A	5′-cacagcccggcGCctggatggcaga-3′
EDR28.l	N350A,D	5′-tccggtactcGHtatcaaggtatt-3′
EDR29.1	R278K,M	5′-tctttatgcgtAWGctgggctcggc-3′

[a] Upper-case bases indicate alterations from the wild-type EntF sequence. D = a, g, or t; K = g or t; N = a, c, g, or t; B = c, g, or t; H = a, c, or t; and W = a or t.

pER311, has a pET28/29-based backbone with N- and C-termini produced using primers EDR1.1 and EDR5.5.

Previously described thioesterase mutants S1138C, D1165A, D1165S, and H1271A were subcloned into pER311 (*22*). Condensation mutants in the isolated C(1−432) domain were generated by sequential PCR using the sense oligonucleotide indicated in Table 1 with its antisense complement and appropriate outside primers and were later subcloned from pER315 into the full-length EntF construct pER311. The exceptions to this procedure were the 18 variants of His-138, which were made first in pER311 in four groups by sequential PCR using EDR19.5 and the sense oligonucleotides indicated in Table 1. For mutants created with degenerate oligonucleotides, multiple colonies were chosen and isolated plasmids were sequenced to obtain the desired mutants.

Protein Expression and Purification. Unless otherwise indicated, agar plates and liquid cultures for cloning and protein expression consisted of Luria−Bertani (LB) media containing 24−50 μg/mL kanamycin. For expression of the C(1−435), C(1−432), and C(1−425) wild-type domains and the C(1−432) mutants, shaker flask cultures of strain BL21-(DE3) (Novagen) transformed with the appropriate plasmid were grown at 37 °C to an OD_{600} of roughly 0.6, induced with 240 μg/mL isopropyl-β-D-thiogalactopyranoside, and incubated an additional 4−5 h prior to centrifugation of the cells and storage at −80 °C. During a typical purification, thawed pellets were resuspended in 12 mL of lysis buffer (50 mM Tris, 2−5 mM imidazole, 300 mM NaCl, pH 8) per liter of culture. After lysis by sonication and removal of cell debris, the C domain was purified by Ni^{2+}-NTA chromatography (Qiagen) using batch binding to 0.6−1.5 mL of resin slurry per 10 mL of lysate, washing with lysis buffer containing 5−10 mM imidazole, and eluting with 300 mM imidazole in lysis buffer. Although the eluted wild-type C(1−432) and C(1−435) domains were >95% pure, for crystallographic purity the C(1−435) protein was loaded onto a Source 15Q anion-exchange column (Pharmacia) in 30 mM Tris, 1 mM dithiothreitol (DTT), and 50 mM NaCl (pH 8), and the protein was eluted in a linear NaCl gradient around 220 mM salt. In addition, the yield and purity of the C(1−432) D142A mutant were so poor that this protein was similarly purified to homogeneity using a Mono Q anion-exchange column (Pharmacia). The isolated C domains were dialyzed against 25 mM Tris, 10 mM $MgCl_2$, 2 mM DTT, and 10% glycerol (pH 8), flash frozen, and stored at −80 °C.

The expression and purification of untagged full-length EntF (*14*), the H1271A mutant (*22*), EntD (*33*), EntE (*19*, *20*), and the EntB aryl carrier protein (EntB-ArCP) (*20*) have been described previously. Cultures for expression of the EntF-His_6 protein and its H138A variant were grown at 30 °C to improve solubility. These two full-length EntF proteins were purified using Ni^{2+}-NTA chromatography in a fashion similar to the isolated C domains. However, lysis buffer was composed of 100 mM Tris (pH 8), 300 mM NaCl, 10 mM $MgCl_2$, and no imidazole; lysis was performed with a French press; the wash buffer contained only 2 mM imidazole; the elution buffer contained only 100 mM NaCl; and the dialysis buffer had 5 mM DTT.

Ser-SNAC Assays of EntF Proteins. Synthesis of L-Ser-SNAC was as described (*30*), and use of this reagent to assay DHB-Ser-SNAC formation by EntF variants was similar to prior work (*30*). Prior to dilution into Ser-SNAC assays, 50−100 μM EntB-ArCP was phosphopantetheinylated by incubation for 45 min at 37 °C in Ent buffer (75 mM Tris, 10 mM $MgCl_2$, 2 mM tris-2-carboxyethylphosphine, pH 7.5) containing 1 mM Coenzyme A and 2.2−3.3 μM EntD. A condensation reaction mix lacking the Ser-SNAC and EntF protein was preincubated for 5 min at 37 °C to enable loading of DHB onto EntB, then the C domain variant was added and condensation was initiated by addition of Ser-SNAC. Final Ser-SNAC reaction mixtures (50 μL) contained Ent buffer, 8 mM ATP, 2.5 mM DHB, 5−10 μM EntB-ArCP, 930 nM EntE, 2 mM L-Ser-SNAC, and 0.5−2.5 μM EntF C domain variant. Reactions were quenched at appropriate times by addition of 50 μL of 0.1 M KOH, the thioester linkage of the DHB-Ser-SNAC product was hydrolyzed by incubation at 60 °C for 4 min, and the reaction was cooled and neutralized with 150 μL of 27 mM formic acid. Proteins were removed by filtration through Ultrafree 5000 NMWL centrifugal filters (Millipore), and the DHB-Ser product was quantitated by HPLC in reference to a standard as previously described (*30*).

In Vitro Assay for Enterobactin Formation. An established ethyl acetate extraction radioassay was used to quantify enterobactin formation in vitro by EntF mutants (*14*, *22*). EntB and EntF were phosphopantetheinylated essentially as described above. Reactions (50 μL) contained Ent buffer, 1 mM [^{3}H]L-serine (46 Ci/mol; Dupont NEN), 1 mM DHB, 10 mM ATP, 10 μM EntB, 0.5−1.0 μM EntE, and 10−3000 nM of EntF variants. Preincubation was performed at 37 °C for 5 min in the absence of EntF, and the EntF protein was added to initiate enterobactin formation. After incubation at 37 °C for appropriate times, the reaction was quenched by addition of 75 μL of 1 N HCl, extracted with 0.4 mL of ethyl acetate, and 0.25 mL of extract was removed and quantified by liquid scintillation counting with 3.5 mL of scintillation fluid.

In Vivo Assay for Enterobactin Formation. The EntF deletion strain ER1100A was generated according to the

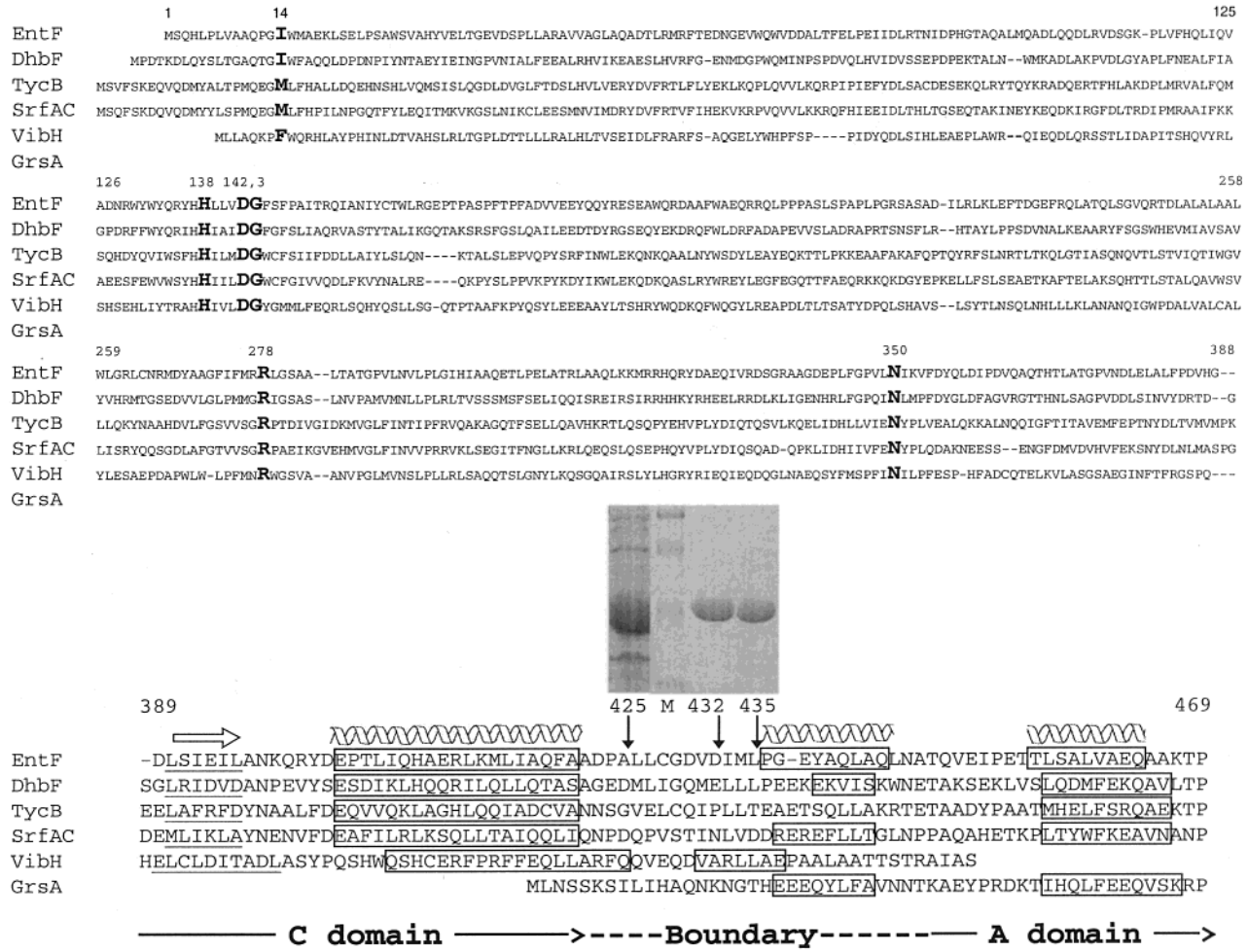

FIGURE 2: Alignment of C domains and C−A boundaries of NRPSs that was used to define the C-terminal boundary of the EntF condensation domain and important active site residues for this activity. The alignment was performed using Clustal_X (*45*) with gap opening and extending penalties of 10 and 2 and included the N-terminal C−A fragments of EntF, the bacillibactin synthetase DhbF, the tyrocidine synthetase TycB, and the surfactin synthetase SrfAC; the naturally free-standing condensation protein VibH; and the A domain of the gramicidin synthetase GrsA that was aligned in a separate step. Secondary structures are indicated for the C−A boundary region by an unfilled arrow for the underlined β-sheet elements and by helices for the boxed α-helical elements and are based on the known VibH and GrsA structures or on predictions by the Jpred server (*46*) for the C−A fragments. Numbers indicate residues of EntF, and bold amino acids correspond to active site mutants made in the EntF C domain. The inserted gel demonstrates that EntF proteins truncated at positions 432 and 435 were purified to homogeneity (final two lanes), while a truncation at position 425 showed expression in a whole-cell lysate (first lane) but yielded no soluble protein. Lane M contained protein markers with molecular weights of 113, 92, 52, and 35 kDa.

protocol of Datsenko and Wanner by amplification of the CAT-containing cassette of pKD3 with primers EDR22.1 and EDR22.2, followed by transformation into strain BW25113/pKD46 and selection for chloramphenicol resistance with loss of ampicillin resistance (*34*). Chrome azurol S (CAS)-containing plates were made as previously described (*35*). Low iron plates were made with M9 minimal media containing 100 μM 2,2′-dipyridyl (Sigma) (*18*). For comparative growth of EntF mutants on low iron plates, liquid cultures of strain ER1100A transformed with appropriate plasmids were grown to saturation in M9 minimal media containing 50 μg/mL kanamycin. The least active EntF mutants grew so poorly in minimal media that they were grown to saturation in LB with 50 μg/mL kanamycin, the cells were pelleted, the LB media were removed, and the pellet was resuspended in minimal media. The resultant saturated minimal media cultures were diluted 10^7-fold with minimal media, and 40 μL of the final dilution was spotted onto low iron plates, leaving ample space between samples to minimize cross-feeding (Figure 6C,D). After brief air-drying, the plates were sealed and incubated at 37 °C for days or weeks until appropriate colony growth was obtained. If the colony size of a condensation mutant was between that of two thioesterase mutants of known activity on the same plate, average colony diameter was determined using a digital photograph (AlphaImager 2200 System, Alpha Innotech) by measuring the five largest, well-isolated colonies for each mutant. A linear logarithmic approximation, diameter $= m_0 + m_1 \cdot \log(\text{activity})$, was used to estimate the activity of the condensation mutant based on its bracketing TE standards.

CD Spectra. The CD spectra of the C(1−432) domain, its mutant variants, and the VibH protein were recorded at a protein concentration of 600 nM in 20 mM Tris (pH 8) at 25 and 37 °C using an AVIV model 60DS spectropolarimeter.

RESULTS

Excision and Characterization of the EntF C Domain. The downstream boundaries of C domains and the upstream

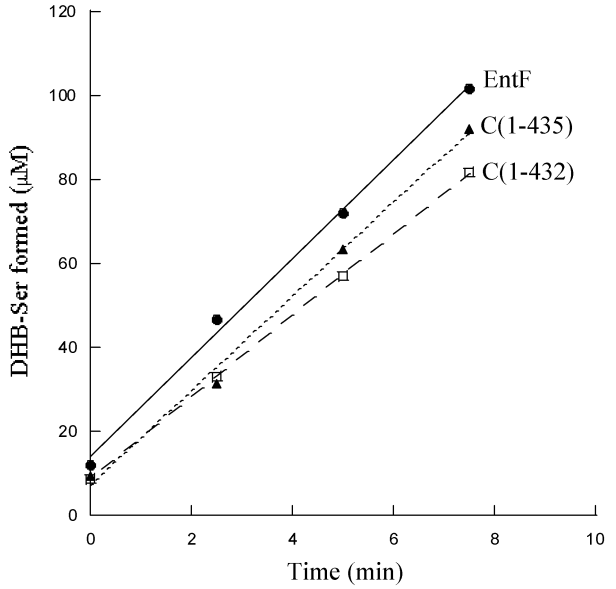

FIGURE 3: Amide bond formation is catalyzed by excised EntF C domains. DHB-*S*-EntB and Ser-SNAC substrates were used to assay 0.5 μM EntF, C(1−432), or C(1−435), and the DHB-Ser product was quantitated by HPLC. Representative data and fits are shown for one set of parallel reactions.

boundaries of A domains in NRPS modules are not exactly known. The predicted domain order of EntF, C−A−PCP−TE, places the amide bond-forming C domain at the N-terminus of the protein, allowing constructs that express just the C domain to be made with one cut at predicted C−A junction sequences. Secondary structure prediction was performed for several C−A domain regions from the N-terminus of large NRPSs. The alignment of these sequences together with the structurally defined adenylation domain of the GrsA protein (*36*) was used to select three sites for expression of N-terminal EntF fragments, at residues 425, 432, and 435 (Figure 2). Constructs that contained a C-terminal His_6 tag were designed for all three cut points and were found to express C domain fragments of appropriate length. However, while the C(1−435) and C(1−432) domains could be purified to homogeneity by Ni^{2+} affinity chromatography, C(1−425) yielded no protein, presumably because of the insolubility of the protein fragment (see gel in Figure 2).

The purified C(1−432) and C(1−435) proteins were assayed for amide bond-forming capacity using L-seryl-SNAC in the presence of phosphopantetheinylated EntB that was loaded with DHB by preincubation with EntE and ATP. Both of the excised C domains formed the DHB-Ser linkage as efficiently as the full-length EntF protein, as shown for one set of parallel incubations in Figure 3. Because the isolated C domains were equivalent in activity, the smaller C(1−432) protein was selected for further characterization. We used CD to directly examine the structure of C(1−432) in comparison to the naturally free-standing C domain VibH (Figure 4A). The CD spectra for the two proteins were nearly identical, suggesting the C domain from within a NRPS module and the naturally isolated C domain have similar overall structures. The extent of ellipticity and lack of sharp minima also indicated well-folded domains with a mix of α-helical and β-sheet secondary structure, in agreement with the crystal structure for VibH that was solved during these

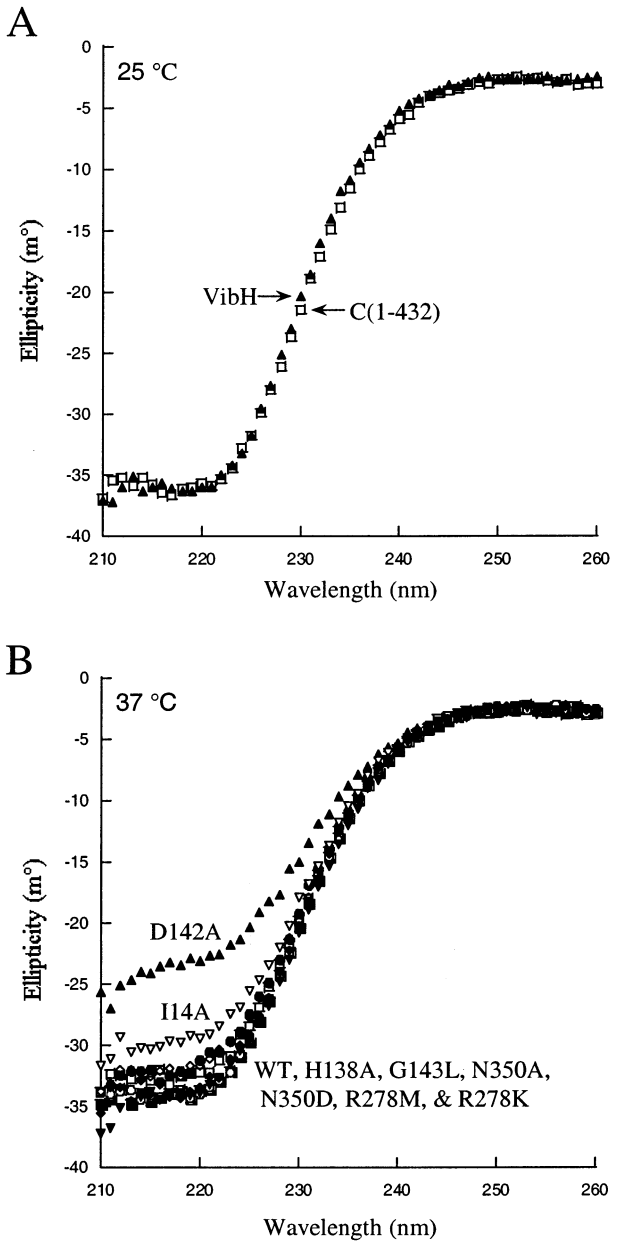

FIGURE 4: CD spectra for (A) VibH and the EntF C(1−432) domain at 25 °C and (B) C(1−432) and its indicated mutant variants at 37 °C.

studies (*29*). Thus, we have successfully isolated a well-folded, fully active, and precisely defined C domain from within a larger nonribosomal peptide synthetase.

DHB-Ser-SNAC Formation and Structural Effects of Active Site Mutations. The isolation of the EntF C domain and the availability of a multiple-turnover assay for its function provided us an excellent framework to probe C domain catalysis in light of the newly solved structure of the VibH protein (Figure 5A) (*29*). The structure of VibH does resemble that of chloramphenicol acetyltransferase (*31*), though with a different oligomeric organization (Figure 5A,B). Modeling of a CAT structure containing substrates over the substrate-free VibH structure suggested residues in the active site that should be important for catalysis if VibH, and by implication EntF C(1−432) and other C domains, function mechanistically like CAT (*24*) (T. A. and A. E. Keating, personal communication) (*29*). Four of these

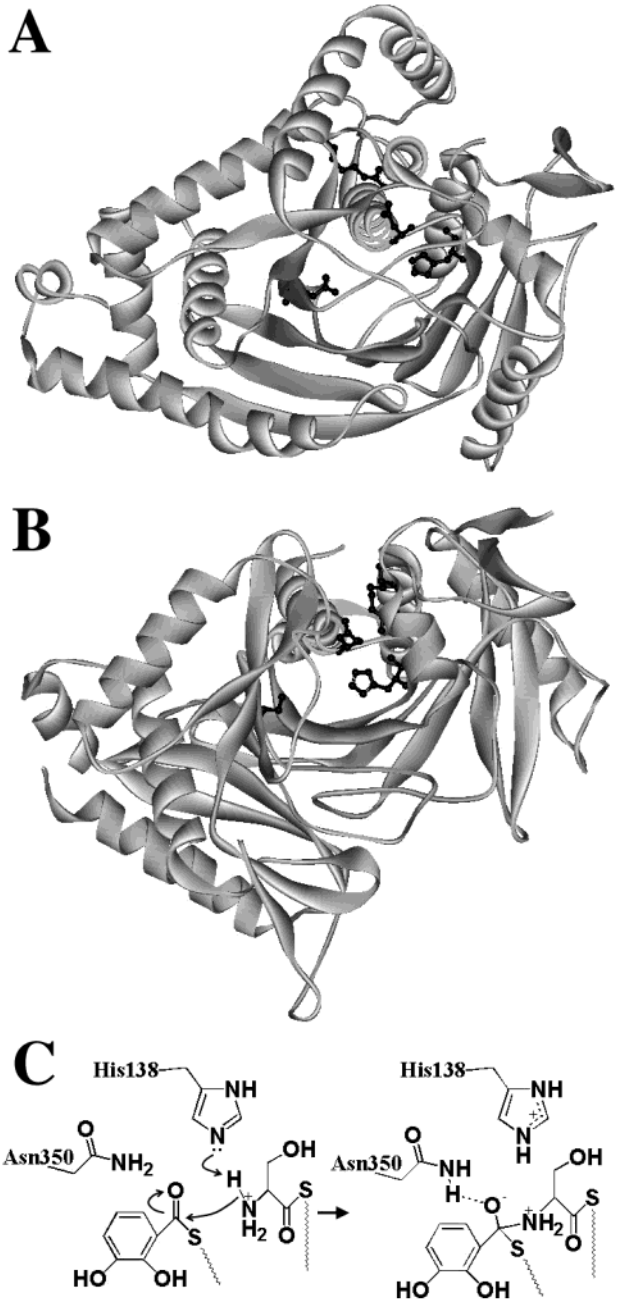

FIGURE 5: Roles in catalysis or active site architecture are proposed for residues of EntF based on the crystal structures of VibH and CAT. (A) The crystal structure of VibH (*29*) in gray ribbon form showing atoms and bonds in black for four active site residues (clockwise from the lower left): Asn-335, Arg-263, Asp-130, and His-126. (B) Gray ribbon diagram showing two of three subunits of trimeric CAT (*31*) constituting one active site interface with corresponding active site residues in black (clockwise from the lower left): Ser-148, Asp-199, Arg-18, and His-195. (C) EntF His-138 is proposed to function as a general base during amide bond formation between DHB and serine. This reaction produces a putative tetrahedral intermediate whose oxyanion may be stabilized by hydrogen bonding with Asn-350.

residues in VibH and their CAT counterparts are shown in Figure 5A,B.

On the basis of this analysis, six residues were selected for mutagenesis in EntF C(1−432) (Figure 2). Histidine 138, the second His of the HHxxxDG motif, was expected to serve as an essential catalytic base to deprotonate the serine amine for attack of this group on the DHB-*S*-EntB thioester carbonyl (Figure 5C) (*25*). The oxyanion of the resulting tetrahedral intermediate would be stabilized by hydrogen bonding to asparagine 350, although the corresponding residue in CATs is a serine (Figure 5C) (*37*). Aspartate 142 of the core motif was not thought to directly participate in catalysis but rather the salt bridge it forms with arginine 278 should be key to the local structure of the active site (*24*, *38*). Although residue 143 appears to have a standard conformation, this motif glycine was mutated to leucine in the belief that the larger side chain would block the active site channel and prevent substrate access (T. A. and A. E. Keating, personal communication). Finally, isoleucine 14 was mutated to alanine despite its lack of strict conservation between C domains because the corresponding conserved tyrosine of CATs packs against and may help to orient the catalytic histidine (*39*). Ultimately, nine mutations were generated among two residues expected to be directly involved in catalysis (His-138 and Asn-350) and four residues believed to have important roles in the local architecture of the active site (Asp-142, Arg-278, Gly-143, and Ile-14).

The nine mutant C(1−432) domains were expressed and purified by Ni^{2+}-NTA chromatography. All yielded protein of sufficient purity for further characterization except for D142A, which gave the lowest yield and required a second round of purification by anion-exchange chromatography. The mutant proteins were assayed for formation of DHB-Ser amide bonds using the Ser-SNAC assay, and averaging of the rates determined from multiple experiments yielded the results shown in Table 2. Only two of the mutant C domains had observable rates of DHB-Ser formation. A conservative mutation of the salt-bridge Arg-278 to Lys had almost no effect on activity, and changing the His-supporting Ile-14 to Ala resulted in a >50-fold decrease in catalysis. All other mutants were inactive to the limit of detection of the Ser-SNAC assay, indicating a >200-fold reduction in catalysis.

The strong effects of the majority of the mutants agreed with their proposed roles in active site catalysis and local structure, but substantial loss of activity could also be caused by mutants that affect the global fold and stability of the C(1−432) domain. To explore this possibility, we examined mutant proteins by CD at the assay temperature of 37 °C. All the mutants tested had similar spectra to the wild-type protein except for I14A, which was marginally reduced in intensity, and D142A, which was substantially reduced in intensity (Figure 4B). The poor expression and weak CD signal observed for the D142A domain indicate that this core motif residue is important for the global fold, not just the local fold, of the EntF C domain. However, the majority of the altered residues, including the putative catalytic mutants, do not appear to significantly affect the overall fold of the C(1−432) domain. The combined results from SNAC assays and CD data are consistent with the proposed roles of side chains in catalysis and structure. Unfortunately, the best assay available to look directly at EntF C domain function (the Ser-SNAC assay) has limited sensitivity, and so to further study these important residues we developed and applied an indirect in vivo assay.

Development of an In Vivo Assay for EntF Function. Whether the condensation reaction is a limiting step for the overall synthesis of enterobactin by wild-type EntF is

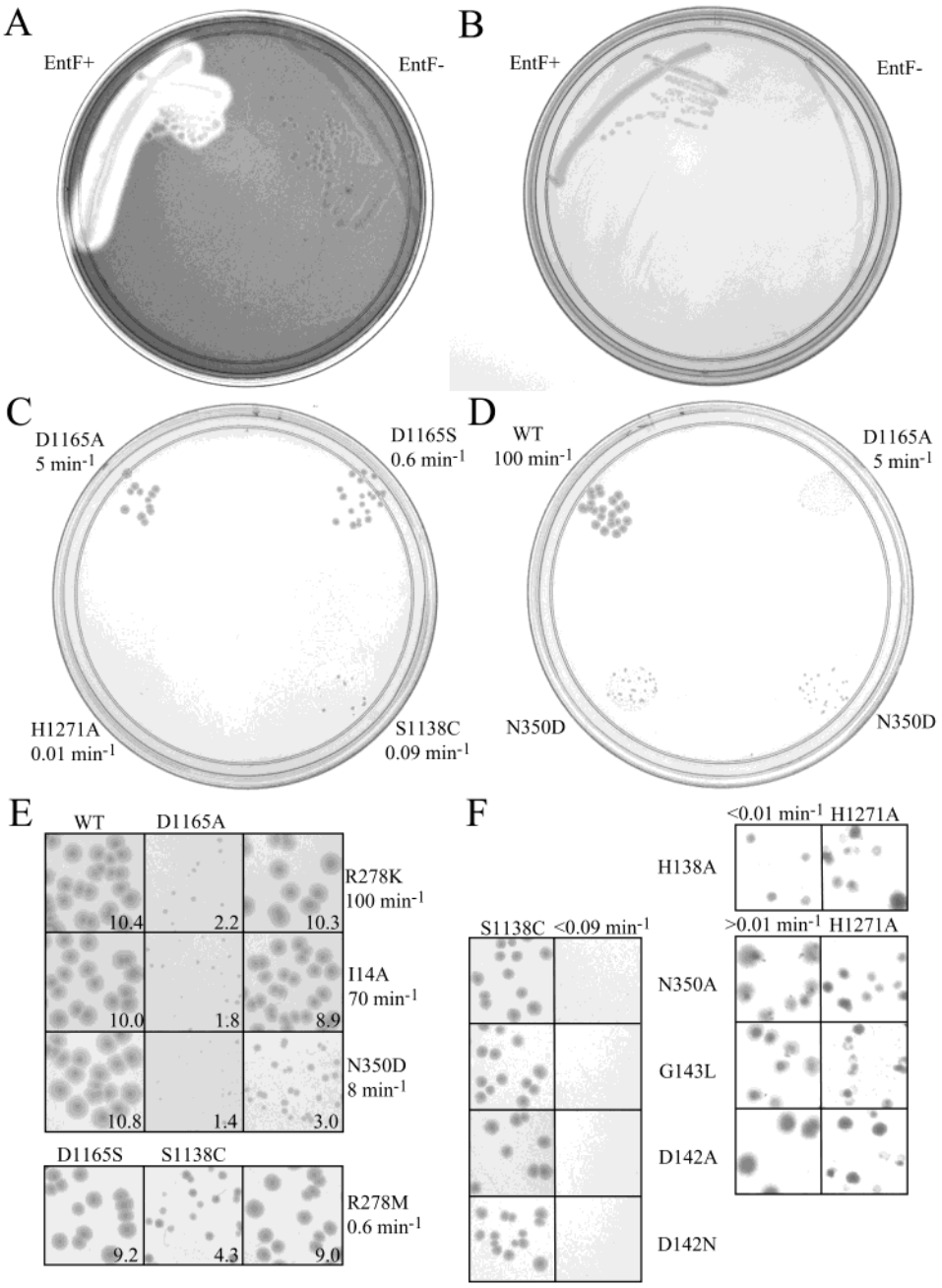

FIGURE 6: In vivo activity measured for mutant variants of EntF. The new EntF$^-$ strain ER1100A was unable to produce enterobactin, as demonstrated by (A) the absence of an iron-depleted halo around ER1100A colonies on a CAS plate (*35*) and (B) the inability of isolated colonies to grow on low iron plates (*18*). (C) Strain ER1100A transformed with the indicated EntF thioesterase mutants exhibited relative growth on low iron plates that correlated with the known in vitro rates of enterobactin synthesis for the TE mutants (*22*). (D) EntF TE mutants of known in vitro activity were used as growth standards to calibrate the growth and therefore activity of EntF condensation mutants. The low iron plate shown placed the colony size of ER1100A transformed with the N350D condensation mutant between that of strains containing wild-type EntF and the D1165A thioesterase mutant. (E) Close-ups of colonies from low iron plate experiments are shown for C mutants whose growth could be bracketed between two TE mutants on the same plate. Each row represents a plate, the first two columns the indicated TE standards, and the third column the condensation mutant named to the right with its activity estimated based on its relative average colony diameter (inset numbers in arbitrary length units). (F) Growth of C mutants with at least a 1000-fold decrease in enterobactin production was measured relative to individual TE standards. These C mutants (middle two columns) with activities below the S1138C TE mutant (first column, 0.09 min^{-1} in vitro) could not be bracketed on the same plate because the H1271A TE mutant (last column, 0.01 min^{-1} in vitro) grew so slowly in comparison to S1138C.

unknown, but this reaction is likely to become limiting in the context of C domain mutants based on their strong defects in amide bond formation observed by SNAC assay. The formation of enterobactin could then be used as an indirect measure of condensation domain function. An in vivo assay for enterobactin production would be particularly appealing, eliminating the need for protein expression and purification for every mutant. The original EntF-defective isolate was undefined in nature and exhibited poor growth even in the presence of iron (unpublished observations) (*18*), so to assay EntF in vivo we first generated a well-defined, robust EntF deletion strain.

The strain ER1100A was made using the technique of Datsenko and Wanner and removes all but the six N-terminal

Table 2: DHB-Ser Amide Bond Formation by Isolated EntF C Domains and Mutants[a]

EntF protein	k_{obs} (DHB-Ser/min)
EntF	21 ± 4
C(1−435)	22 ± 8
C(1−432)	24 ± 6
R278K	15 ± 1
I14A	0.34 ± 0.04
N350D	<0.1
R278M	<0.1
N350A	<0.1
D142A	<0.1
H138A	<0.1
H138E	<0.1
G143L	<0.1

[a] Average values given ± standard deviation were determined using 3−6 independent experiments. The mutants were assayed as C(1−432) domain fragments. Ser-SNAC assays were performed at 0.5 μM for EntF, C(1−435), C(1−432), and R278K; and at 2.5 μM for the other mutants.

and six C-terminal codons of EntF, replacing the intervening sequence with a cassette containing a CAT gene (*34*). The inability of this strain to produce enterobactin was confirmed by two plate assays. Special minimal media plates containing a complex of the dye chrome azurol S (CAS) with iron(III) are an opaque blue, but bacterial colonies that secrete siderophores will take up the iron from the complex, leading to clear yellow halos around the siderophore-producing colonies (*35*). Figure 6A shows that while the wild-type parent strain produced a halo on a CAS plate, colonies of the EntF deletion strain had no halo because of their failure to produce enterobactin. Likewise, when the wild-type and EntF-defective strains were streaked on minimal media plates that contained the iron chelator 2,2′-dipyridyl (*18*), isolated colonies were present for the parent strain but failed to grow for the enterobactin nonproducer ER1100A under the iron-poor conditions (Figure 6B).

The differential growth of EntF-defective cells on dipyridyl low iron plates provided an assay for rough quantitative measurement of activity for various EntF mutants. Previously, rates of enterobactin formation in vitro were measured for full-length EntF proteins with mutations in the Ser−His−Asp catalytic triad of the thioesterase (TE) domain, the final domain of EntF (Figure 1A) (*22*). Appropriate dilutions of strain ER1100A transformed with the various TE mutants of EntF were spotted on low iron plates and incubated at 37 °C. The relative growth of the different TE-mutant strains correlated exactly with their known in vitro rates for enterobactin formation (Figure 6C). This suggested that the TE-mutant strains could be used as calibration standards to estimate the activity of strains containing C domain mutants in the complete EntF protein. In addition, while growth of the H1271A mutant could not be detected within the same time frame as the other thioesterase mutants (Figure 6C), H1271A cells grew faster than cells entirely lacking EntF (data not shown). This result makes the in vivo assay highly sensitive, as H1271A forms enterobactin in vitro at a rate approximately 10 000-fold below WT (roughly 0.01 and 100 min^{-1}, respectively) (*22*).

In Vivo Assay of Condensation Mutants. EntF-defective cells transformed with full-length EntF constructs containing C domain mutants were spotted individually on low iron plates in comparison to the TE-mutant strains with the most similar level of activity. For example, the N350D condensation domain mutant was compared to wild-type EntF and the most active thioesterase mutant, D1165A, because its rate of growth clearly falls between the two (Figure 6D). This bracketing strategy was followed for the four C domain mutants that had the highest activity in vivo. The average colony diameter was determined for each C domain mutant along with the corresponding TE standards and used to roughly estimate the activity of the condensation mutant. The results are shown in Figure 6E, with close-ups of the spotted TE standards in the first two columns, the C domain mutant in the third column, and each row of close-ups coming from the same low iron plate. A conservative mutation of the salt bridge Arg-278 to Lys had no effect on activity, but changing the residue to Met reduced enterobactin formation by roughly 200-fold. Mutation of the His-supporting Ile-14 to Ala had little effect, and changing the putative intermediate-stabilizing Asn-350 to Asp caused about a 10-fold decrease in enterobactin synthesis. The modest reduction in enterobactin production observed in vivo for the I14A and N350D mutants (Figure 6E) contrasts with their loss of condensation activity measured in vitro through formation of DHB-Ser-SNAC (Table 2).

The remaining C domain mutants could not be bracketed because of the disparate growth rates of the corresponding TE standards. However, comparison to single TE standards indicated that the N350A, G143L, and D142A mutations all reduced enterobactin synthesis by between 3 and 4 orders of magnitude (Figure 6F). The H138A mutation of the putative catalytic base was the only construct that caused a more than 10 000-fold decrease in activity (Figure 6F). The importance of residue 138 was further probed by the construction of a library at this position encoding all of the natural amino acids except for tryptophan. When the H138 mutants were streaked on low iron plates, only the H138K mutant showed significant growth of isolated colonies, similar to the roughly 1000-fold defective TE standard S1138C (data not shown).

Activity and Complementation of H138A EntF In Vitro. The H138A full-length EntF protein was expressed, purified, and assayed for enterobactin formation in vitro in comparison to the H1271A thioesterase mutant (Figure 7). The averaged turnover rates were roughly 0.01 min^{-1} for both H138A and H1271A, but the C domain mutant was consistently just below the TE mutant in every individual comparison, in agreement with the in vivo results. We then asked whether the H138A EntF protein could be complemented in trans, either by the isolated C(1−432) domain or by H1271A EntF. Addition of C(1−432) raised the rate to 0.07 min^{-1}, and the mixture of H138A and H1271A gave a rate of 0.13 min^{-1}. These slight enhancements may indicate some weak in trans catalysis or intermediate transfer but are still 2−3 orders of magnitude below WT activity, here observed at the low end of its range (60−200 min^{-1}).

DISCUSSION

We have tested the importance of several active site side chains for catalysis by the EntF condensation domain and have observed strong effects for several mutations with assays in vitro and in vivo. At first glance, some of the results for the in vitro production of DHB-Ser-SNAC by C(1−432)

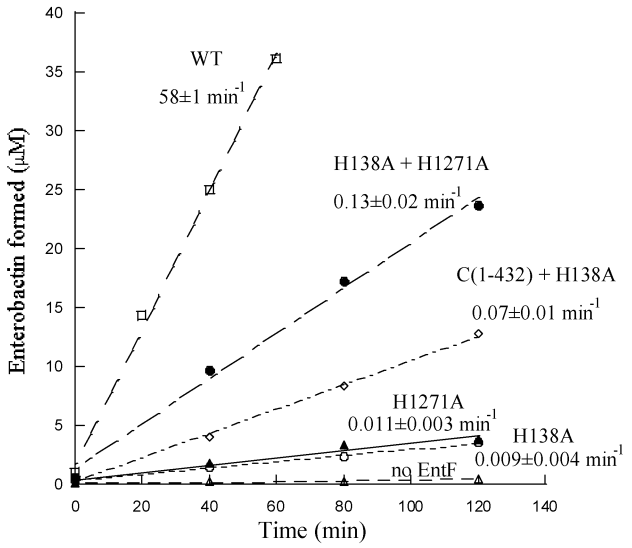

FIGURE 7: Enterobactin production in vitro by wild type (10 nM, His_6 tagged, open squares), H1271A (3 μM, filled triangles), H138A (3 μM, open circles), C(1−432) + H138A (1.5 μM each, open diamonds), H1271 + H138A (1.5 μM each, filled circles), or no EntF (open triangles). The assay was based on ethyl acetate extraction of radiolabeled serine (*22*).

mutants seem to contrast with in vivo production of complete enterobactin by full-length EntF mutants. The I14A folding mutant was more than 50-fold defective by SNAC assay but barely affected in vivo production of enterobactin, and the N350D mutant produced less than 1/200 as much DHB-Ser-SNAC as wild type but made only 10-fold less enterobactin. These results could be explained if amide bond formation by the EntF C domain is not normally a limiting step in the overall production of enterobactin. Only when condensation activity is reduced more than 50-fold might it begin to have an affect on the overall rate of enterobactin production by EntF. If this conclusion is true, the in vivo assay most likely underestimates the effect of mutations on condensation activity by an order of magnitude, even after accounting for three condensation events for each enterobactin molecule formed (Figure 1).

Assuming this shortfall, elimination of the side chain of His-138 reduced EntF C domain activity by about 5 orders of magnitude without affecting the global fold, similar to the change in k_{cat} for chloramphenicol acetyl transferase caused by mutagenesis of its catalytic histidine (*25*). This is the strongest effect reported for histidine mutation of a C domain and agrees well with the homologous active site structures observed for the VibH condensation domain and the type III CAT (Figure 5A,B). However, mutation of the corresponding histidine in VibH itself had essentially no affect on activity (*29*). This surprising result indicates that despite the similar positioning and orientation of the residue, VibH does not require the general base that is essential for CAT activity (*25*). Mixed results have also been obtained for the vibriobactin synthetase VibF that performs two condensation steps, one of which is 1000-fold affected but the other only 9-fold altered by absence of the corresponding histidine (*26*). The lack of His dependence seen for the vibriobactin synthetases seems likely to represent only a small subset of NRPS condensation domains (perhaps those that use free amines rather than aminoacyl-*S*-PCP intermediates as acceptor substrates) because this residue is highly conserved among NRPS C domains. Indeed, cognate histidine mutations in the first C domain of tyrocidine synthetase B (TycB) cause at least a 2 orders of magnitude drop in activity (*27*, *28*). Thus, the EntF C domain and most likely the majority of NRPS condensation domains depend on this catalytic residue in the same manner as chloramphenicol acetyl transferase (Figure 5C) (*24*).

The importance of His-138 to EntF C domain catalysis is also demonstrated by the inability of 18 other residues to effectively replace it according to the in vivo assay (data not shown). Only H138K showed a significant retention of activity, roughly an order of magnitude up from the Ala substitution but still 3−4 orders of magnitude below wild type. Presumably, some level of deprotonated lysine is present and able to serve, albeit poorly, as a general base for the EntF C domain. For CAT, a mutation of the catalytic His to Glu produced an elevated pK_a for Glu, and the mutant retained a 10-fold greater activity than other His substitutions (*25*). Glutamate had no such effect in vitro or in vivo for EntF.

The VibH structure suggested that a second residue may be directly involved in C domain catalysis, an asparagine positioned to serve as a hydrogen bond donor for stabilization of the tetrahedral intermediate generated during amide bond synthesis (Figure 5A,C). An Asn→Leu mutation in VibH had only slight effects on k_{cat} and K_m values (*29*). For EntF, change of Asn-350 to Asp and to Ala reduced product formation greater than 200 (SNAC assay) and 1000-fold (in vivo), respectively, without affecting the overall structure. Stabilization of the tetrahedral intermediate in CAT is attributed to a serine residue for which a change to alanine reduces k_{cat} 53-fold without affecting K_m values (*37*). This CAT Ser cannot be changed to Asn without even greater reduction in activity, but for the serine protease subtilisin the related oxyanion intermediate is stabilized by hydrogen bonding to an asparagine (*37*, *40*). Our results provide the first kinetic evidence in support of a similar catalytic role for an asparagine in C domain function.

The importance of an Asp−Arg salt bridge to the C domain active site structure is further supported by our data. A conservative R278K mutation did not significantly affect EntF activity, while a R278M change caused at least a 200-fold defect without substantially disrupting the global structure. The D142A mutation not only greatly reduced amide bond formation but disrupted the overall fold of the protein. These results are in reasonable agreement with data for CAT, where Arg→Val and Asp→Ala mutations each reduce k_{cat} an order of magnitude, and the Asp→Ala mutant is thermolabile (*38*). A CAT Asp→Asn mutant is thermostable but is thought to alter the active site architecture, leading to a 1500-fold reduced k_{cat} (*38*). Mutations in other C domains also support the importance of the motif aspartate. For VibH, a 300-fold decrease in k_{cat} resulted from an Asp→Ala mutation that did not appear to affect the overall structure according to CD (*29*). A TycB Asp→Asn mutation eliminated condensation, although the salt-bridge Arg→Ala mutation did not affect activity (*27*). In vivo, a chromosomal point mutation changing Asp→Ala in the SrfA-B synthetase abolished production of the antibiotic surfactin (*41*). Despite all the data indicating the importance of the motif aspartate for catalysis, the VibH and CAT structures clearly indicate that the role is indirect and involves no contact to the catalytic

His side chain, ruling out catalytic diad models where Asp directly alters the His pK_a (*24*, *29*).

Mutation of the motif Gly-143→Leu reduced activity of the EntF C domain in vivo by at least 3 orders of magnitude, placing it in a similar class with the catalytic residues His-138 and Asn-350. The weak synthesis of enterobactin by G143L is presumed to result from poor substrate access to a blocked active site channel, and this mutant could be useful for studies of substrate interaction with the EntF condensation domain. Intriguingly, like the catalytic His and Asn mutants, a corresponding Gly→Leu mutation in VibH has essentially no effect on condensation (*29*). Thus, three active site residues that appear to be central and essential to EntF activity are dispensable for VibH. These results point to the danger of assuming, in the absence of kinetic data, that proteins of similar structure make similar use of active site side chains for catalysis.

The poor complementation of H138A EntF in trans by either the isolated EntF C(1−432) domain or the full-length H1271A EntF supports a monomeric functional state for EntF and most other NRPS systems (Figure 7). The organizationally similar polyketide synthases are dimeric, and the mixing of two variants of the same synthetase with mutations in different functional domains allows reconstitution of near wild-type activity for these systems (*42*, *43*). The inability of EntF mutants H138A and H1271A to effectively combine suggests that neither the C nor the TE domain of EntF is able to efficiently use the PCP from a different subunit. Attempts to isolate EntF fragments lacking the C domain and so encoding just A−PCP−TE produced proteins with K_m values for serine that were roughly 2 orders of magnitude higher than WT (data not shown). Therefore, we could not test whether the failure of the C(1−432) domain to complement H138A EntF in trans was due to steric blocking from the presence of an inactive C domain or to the lack of a direct linkage. Nonetheless, these data support a monomeric state for NRPSs, as verified recently by ultracentrifugation of EntF and biochemical studies of other NRPSs (*44*).

The functional C-terminal boundary of an NRPS C domain from within a larger synthetase was defined by this study. The results are particularly useful in light of the VibH structure because the C-terminal helix of the VibH C domain and the N-terminal helix of the A domain from GrsA appear to correspond in protein alignments of C−A junctions (Figure 2). In the case of VibH, which naturally has no downstream domain, this helix is somewhat disordered and at the surface of the protein (Figure 5A, helix furthest to the left; T. A. Keating, personal communication). GrsA is an initiation module with no upstream domain, and the specified helix rests against the surface of the A domain and is preceded by a long loop (*36*). Therefore, it is unclear based on the structures alone whether this helix is required for function of either domain in the context of a C−A boundary of a megasynthetase. The unaltered activity of the EntF C(1−432) and C(1−435) proteins indicates that this helix is not required for C domain catalysis and so is likely to be required either for A domain function or as a structural element for orienting the two domains in the larger synthetase. The linker between this interesting helix and the preceding helix of the C domain also appears to have many residues with a conserved hydrophobic or polar character, contrasting with other interdomain linkers and suggesting that this element may also be important for orienting the two domains (Figure 2, unpublished results). Condensation domains are typically followed by adenylation domains within megasynthetases, and the knowledge gained here should facilitate efforts to generate new products by swapping domains or modules between NRPSs using linkages formed at C−A boundaries.

The reagents and assays we have developed should also prove fruitful for future studies of specificity and interdomain interactions in NRPSs. The EntF C domain has been demonstrated to have specificity for serine as the downstream substrate (*30*). The isolated C(1−432) domain offers an excellent candidate for structural studies in the presence of small-molecule and PCP-tethered substrates to examine acyl intermediate−C domain contacts and protein−protein interactions. The in vivo system used here for assay of EntF will empower selection of mutant and domain-swapped EntF proteins, allowing discovery of residues that contribute to substrate specificity and interdomain recognition for all four of the core NRPS domains included in the EntF protein. The first effective genetic system for study of NRPSs should advance our capacity to design NRPS assembly lines to produce new compounds with therapeutic value.

ACKNOWLEDGMENT

We are grateful to Thomas Keating, Amy Keating, and C. Gary Marshall for sharing results prior to publication and assistance in preparing this manuscript, and David Ehmann and John Trauger for some of the reagents used in these studies.

REFERENCES

1. Crosa, J. H., and Walsh, C. T. (2002) *Microbiol. Mol. Biol. Rev. 66*, 223−49.
2. Schwarzer, D., and Marahiel, M. A. (2001) *Naturwissenschaften 88*, 93−101.
3. Cane, D. E., and Walsh, C. T. (1999) *Chem. Biol. 6*, R319−25.
4. Keating, T. A., and Walsh, C. T. (1999) *Curr. Opin. Chem. Biol. 3*, 598−606.
5. Keller, U., and Schauwecker, F. (2001) *Prog. Nucleic Acid Res. Mol. Biol. 70*, 233−89.
6. Doekel, S., and Marahiel, M. A. (2000) *Chem. Biol. 7*, 373−84.
7. Linne, U., Doekel, S., and Marahiel, M. A. (2001) *Biochemistry 40*, 15824−34.
8. Mootz, H. D., Schwarzer, D., and Marahiel, M. A. (2000) *Proc. Natl. Acad. Sci. U.S.A. 97*, 5848−53.
9. Schneider, A., Stachelhaus, T., and Marahiel, M. A. (1998) *Mol. Gen. Genet. 257*, 308−18.
10. Schwarzer, D., Mootz, H. D., and Marahiel, M. A. (2001) *Chem. Biol. 8*, 997−1010.
11. Stachelhaus, T., Schneider, A., and Marahiel, M. A. (1996) *Biochem. Pharmacol. 52*, 177−86.
12. Miller, D. A., Luo, L., Hillson, N., Keating, T. A., and Walsh, C. T. (2002) *Chem. Biol. 9*, 333−44.
13. Keating, T. A., Marshall, C. G., and Walsh, C. T. (2000) *Biochemistry 39*, 15522−30.
14. Gehring, A. M., Mori, I., and Walsh, C. T. (1998) *Biochemistry 37*, 2648−59.
15. Patel, H. M., and Walsh, C. T. (2001) *Biochemistry 40*, 9023−31.
16. Gaitatzis, N., Kunze, B., and Muller, R. (2001) *Proc. Natl. Acad. Sci. U.S.A. 98*, 11136−41.
17. Young, I. G., Langman, L., Luke, R. K., and Gibson, F. (1971) *J. Bacteriol. 106*, 51−7.
18. Luke, R. K., and Gibson, F. (1971) *J. Bacteriol. 107*, 557−62.
19. Rusnak, F., Faraci, W. S., and Walsh, C. T. (1989) *Biochemistry 28*, 6827−35.
20. Gehring, A. M., Bradley, K. A., and Walsh, C. T. (1997) *Biochemistry 36*, 8495−503.

21. Reichert, J., Sakaitani, M., and Walsh, C. T. (1992) *Protein Sci. 1*, 549−56.
22. Shaw-Reid, C. A., Kelleher, N. L., Losey, H. C., Gehring, A. M., Berg, C., and Walsh, C. T. (1999) *Chem. Biol. 6*, 385−400.
23. De Crecy-Lagard, V., Marliere, P., and Saurin, W. (1995) *C. R. Acad. Sci. III 318*, 927−36.
24. Murray, I. A., and Shaw, W. V. (1997) *Antimicrob. Agents Chemother. 41*, 1−6.
25. Lewendon, A., Murray, I. A., Shaw, W. V., Gibbs, M. R., and Leslie, A. G. (1994) *Biochemistry 33*, 1944−50.
26. Marshall, C. G., Hillson, N. J., and Walsh, C. T. (2002) *Biochemistry 41*, 244−50.
27. Bergendahl, V., Linne, U., and Marahiel, M. A. (2002) *Eur. J. Biochem. 269*, 620−9.
28. Stachelhaus, T., Mootz, H. D., Bergendahl, V., and Marahiel, M. A. (1998) *J. Biol. Chem. 273*, 22773−81.
29. Keating, T. A., Marshall, C. G., Walsh, C. T., and Keating, A. E. (2002) *Nat. Struct. Biol. 9*, 522−6.
30. Ehmann, D. E., Trauger, J. W., Stachelhaus, T., and Walsh, C. T. (2000) *Chem. Biol. 7*, 765−72.
31. Leslie, A. G., Moody, P. C., and Shaw, W. V. (1988) *Proc. Natl. Acad. Sci. U.S.A. 85*, 4133−7.
32. Parsell, D. A., Silber, K. R., and Sauer, R. T. (1990) *Genes Dev. 4*, 277−86.
33. Lambalot, R. H., Gehring, A. M., Flugel, R. S., Zuber, P., LaCelle, M., Marahiel, M. A., Reid, R., Khosla, C., and Walsh, C. T. (1996) *Chem. Biol. 3*, 923−36.
34. Datsenko, K. A., and Wanner, B. L. (2000) *Proc. Natl. Acad. Sci. U.S.A. 97*, 6640−5.
35. Schwyn, B., and Neilands, J. B. (1987) *Anal. Biochem. 160*, 47−56.
36. Conti, E., Stachelhaus, T., Marahiel, M. A., and Brick, P. (1997) *EMBO J. 16*, 4174−83.
37. Lewendon, A., Murray, I. A., Shaw, W. V., Gibbs, M. R., and Leslie, A. G. (1990) *Biochemistry 29*, 2075−80.
38. Lewendon, A., Murray, I. A., Kleanthous, C., Cullis, P. M., and Shaw, W. V. (1988) *Biochemistry 27*, 7385−90.
39. Murray, I. A., Lewendon, A., and Shaw, W. V. (1991) *J. Biol. Chem. 266*, 11695−8.
40. Robertus, J. D., Kraut, J., Alden, R. A., and Birktoft, J. J. (1972) *Biochemistry 11*, 4293−303.
41. Vollenbroich, D., Kluge, B., D'Souza, C., Zuber, P., and Vater, J. (1993) *FEBS Lett. 325*, 220−4.
42. Kao, C. M., Pieper, R., Cane, D. E., and Khosla, C. (1996) *Biochemistry 35*, 12363−8.
43. Staunton, J., Caffrey, P., Aparicio, J. F., Roberts, G. A., Bethell, S. S., and Leadlay, P. F. (1996) *Nat. Struct. Biol. 3*, 188−92.
44. Sieber, S. A., Linne, U., Hillson, N., Roche, E. D., Walsh, C. T., and Marahiel, M. A. (2002) *Chem. Biol. 9*, 997−1008.
45. Thompson, J. D., Gibson, T. J., Plewniak, F., Jeanmougin, F., and Higgins, D. G. (1997) *Nucleic Acids Res. 25*, 4876−82.
46. Cuff, J. A., Clamp, M. E., Siddiqui, A. S., Finlay, M., and Barton, G. J. (1998) *Bioinformatics 14*, 892−3.

BI026867M